Hindawi Publishing Corporation
Journal of Chemistry
Volume 2014, Article ID 546956, 6 pages
http://dx.doi.org/10.1155/2014/546956

Research Article

Fabrication of γ-Fe_2O_3 Nanoparticles by Solid-State Thermolysis of a Metal-Organic Framework, MIL-100(Fe), for Heavy Metal Ions Removal

Shengtao Hei, Yan Jin, and Fumin Zhang

Key Laboratory of the Ministry of Education for Advanced Catalysis Materials, Institute of Physical Chemistry, Zhejiang Normal University, Jinhua 321004, China

Correspondence should be addressed to Fumin Zhang; fumin.zhang@gmail.com

Received 27 May 2014; Accepted 8 August 2014; Published 18 August 2014

Academic Editor: Ackmez Mudhoo

Porous γ-Fe_2O_3 nanoparticles were prepared via a solid-state conversion process of a mesoporous iron(III) carboxylate crystal, MIL-100(Fe). First, the MIL-100(Fe) crystal that served as the template of the metal oxide was synthesized by a low-temperature (<100°C) synthesis route. Subsequently, the porous γ-Fe_2O_3 nanoparticles were fabricated by facile thermolysis of the MIL-100(Fe) powders via a two-step calcination treatment. The obtained γ-Fe_2O_3 was characterized by X-ray diffraction (XRD), N_2 adsorption, X-ray photoelectron spectroscopy (XPS), and scanning electron microscopy (SEM) techniques, and then used as an adsorbent for heavy metal ions removal in water treatment. This study illustrates that the metal-organic frameworks may be suitable precursors for the fabrication of metal oxides nanomaterials with large specific surface area, and the prepared porous γ-Fe_2O_3 exhibits a superior adsorption performance for As(V) and As(III) ions removal in water treatment.

1. Introduction

As(V) and As(III) are considered as primarily highly toxic pollutants in water resources due to their wide spread use in industrial processes, and their efficient removal from water is of great importance. A number of strategies have been applied in order to remove these contaminants from wastewater [1]. Among them, adsorption-based removal technique is one of the most widely investigated methods because of its availability, profitability, ease of operation, and efficiency in comparison with other methods [2]. So far, a variety of arsenic adsorbents have been evaluated, among which the granules of iron oxides or hydroxides exhibit high adsorption capacities and have made them the most commonly utilized adsorbents for the removal of the arsenic contaminants [3–24]. However, fabrication of the porous γ-Fe_2O_3 nanoparticles with a high specific surface area that favors a high adsorption capacity, as well as the separation of the saturated adsorbents so as to prevent secondary pollution during their usage, is still a challenging topic.

Recently, metal-organic frameworks (MOFs) with diverse architectures and morphologies have been recognized as promising precursors/templates to develop the porous iron oxides [25–32]. For example, Xu and coworkers reported the fabrication of spindle-like mesoporous α-Fe_2O_3 using MOF MIL-88(Fe) as template [25]. Their prepared spindle-like mesoporous α-Fe_2O_3 was composed of clustered Fe_2O_3 nanoparticles with size of <20 nm. Zhang and coworkers demonstrated a facile synthesis of porous Fe_2O_3 nanocubes by simultaneous oxidative decomposition of Prussian blue nanocubes [32]. The derived porous Fe_2O_3 nanocubes are composed of very fine Fe_2O_3 nanoparticles with size of several nanometers. It should be stressed that, MOFs show distinct advantages due to their well-ordered crystalline structure, high porosity, large surface area, and tunable pore size, in comparison with other templates. However, facile and controlled synthesis of magnetic nanoparticles γ-Fe_2O_3 from the thermolysis of Fe-based MOFs, is still rarely reported.

MIL-100(Fe), a novel mesoporous MOF, has a large BET specific surface area and pore volume with the presence of a significant amount of accessible Lewis acid metal sites upon dehydration [33, 34]. Considering that the synthesis and application of MIL-100(Fe) is an area of much interest

and still in its infancy, in the current work, we synthesized the MIL-100(Fe) crystals at low temperature and atmospheric pressure conditions, and then fabricated the porous γ-Fe_2O_3 nanoparticles by simple thermolysis of the obtained MIL-100(Fe) powders via a two-step calcination treatment. Compared to the ordinary γ-Fe_2O_3 materials obtained by a solvothermal process and subsequent calcination, this strategy is simple, inexpensive, and scalable. When the prepared porous γ-Fe_2O_3 nanoparticles were used as adsorbent in water treatment, this magnetic material showed an excellent performance for heavy metal ion removal.

2. Experimental Section

2.1. Preparation of the Porous γ-Fe_2O_3. The template, MIL-100(Fe), was prepared by a facile low-temperature (<100°C) synthesis route according to the procedure described in our previous work [35]. Afterwards, the MIL-100(Fe) powders were placed in a tube furnace under N_2 gas flow (1° min^{-1}), heated to 450°C, and maintained at 450°C for 2 h. Then the resulting black powders were placed in a box furnace, and heated to 450°C (1° min^{-1}), and maintained at 450°C for 2 h in air. This two-step calcination resulted in the final porous γ-Fe_2O_3 nanoparticles.

2.2. Characterization. The X-ray powder diffraction (XRD) patterns were obtained on a Philips PW3040/60 diffractometer, using Cu$K\alpha$ radiation (λ = 0.1541 nm) in a scanning range of 3 to 50° at a scanning rate of 1° min^{-1}. N_2 adsorption isotherms were obtained at −196°C using a Micromeritics ASAP 2020 instrument. The samples were outgassed under vacuum at 150°C for 10 , prior to the adsorption measurements. The scanning electron microscope (SEM) observations were performed on a Hitachi S-4800 apparatus equipped with a field emission gun. The transmission electron microscopy (TEM) observations were carried out on a JEOL JEM-1200 working at 120 kV. The surface electronic states of the synthesized samples were investigated by X-ray photoelectron spectroscopy (XPS, Thermo Scientific EscaLab 250Xi using Al$K\alpha$ radiation). The XPS data were internally calibrated fixing the binding energy of C 1s at 284.6 eV.

2.3. Water Treatment Experiment. Solutions containing different concentrations of As(V) and As(III) were prepared using $NaH_2AsO_4{\cdot}12H_2O$ and As_2O_3 as the sources of heavy metal ions, respectively. To obtain the adsorption isotherms, 10 mg of γ-Fe_2O_3 was added to the above solution under stirring at room temperature. After the specified time, the solid and liquid were separated and an IRIS Intrepid IIXSP inductively coupling plasma-atomic emission spectrometer (ICP-AES) was used to measure the concentration of metal ions in the remaining solution.

3. Results and Discussion

The XRD patterns of the template MIL-100(Fe) (Figure S1 in Supplementary data available online at http://dx.doi.org/10.1155/2014/546956) are very similar with the simulated ones

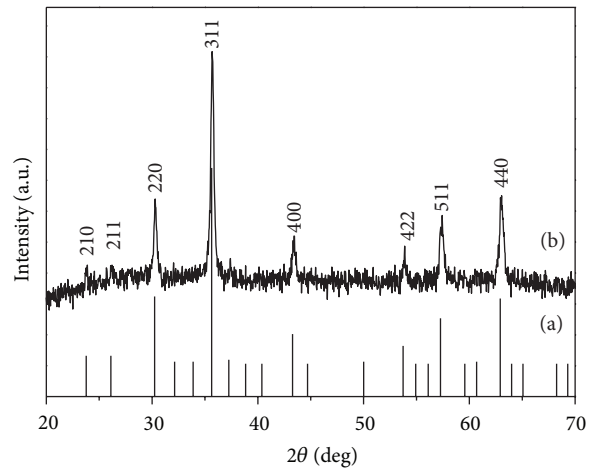

Figure 1: XRD patterns of the simulated γ-Fe_2O_3 (a) and the prepared γ-Fe_2O_3 (b).

reported in literature [33, 34], confirming the formation of the metal-organic framework. Figure 1 illustrates the XRD patterns of the sample derived from MIL-100(Fe) via the so-called two-step calcination treatment. It can be observed that all the diffraction peaks can be assigned to γ-Fe_2O_3 with a cubic structure (JCPDS card no. 39-1346) [32]. No peak from any impurities can be observed in the XRD patterns, indicating high purity of γ-Fe_2O_3 products, and also the template was completely transformed into γ-Fe_2O_3 after the two-step calcination. Estimated grain size of the sample using Scherrer equation was about 30 nm. SEM and TEM images show that the γ-Fe_2O_3 nanomaterial is made of nano-aggregates with a relatively homogeneous particle sized distribution between 20 and 50 nm (Figures S2 and S3 in Supplementary data), in accordance with the result calculated by Scherrer equation.

The chemical composition of the template MIL-100(Fe) and the derived γ-Fe_2O_3 were further characterized by using XPS. The XPS spectra of MIL-100(Fe) (Figure S4 in Supplementary data) are almost identical to those of Fe-BTC, the counterpart of MIL-100(Fe) [36]. The XPS spectra of the derived γ-Fe_2O_3 are shown in Figure 2(a). The predominant elements are Fe and O, and small amounts of residual C are also present. The peaks at binding energy of 56, 284.6, and 530.4 eV were designated for Fe3p3/2, C1s, and O1s, respectively. High resolution XPS of Fe2p is shown in Figure 2(b). Binding energy of Fe2p1/2 is 724.8 eV and binding energy of Fe2p3/2 is 711.1 eV. The presence of satellite peak at 719 eV is characteristic for maghemite. These results agree with literature values of the γ-Fe_2O_3 particles [2].

For the template MIL-100(Fe), its specific surface area and total pore volume are 1800 m^2 g^{-1} and 1.0 cm^3 g^{-1}, respectively, estimated by N_2 adsorption and desorption (Figure S5(a) in Supplementary data). The pore size distribution curve of the MIL-100(Fe) sample displays two different pore sizes centered at about 1.9 and 2.2 nm (Figure S5(b) in Supplementary data) confirming the presence of the two types of mesoporous cages in MIL-100(Fe) [33]. The N_2 analysis also demonstrates the mesoporous character of the

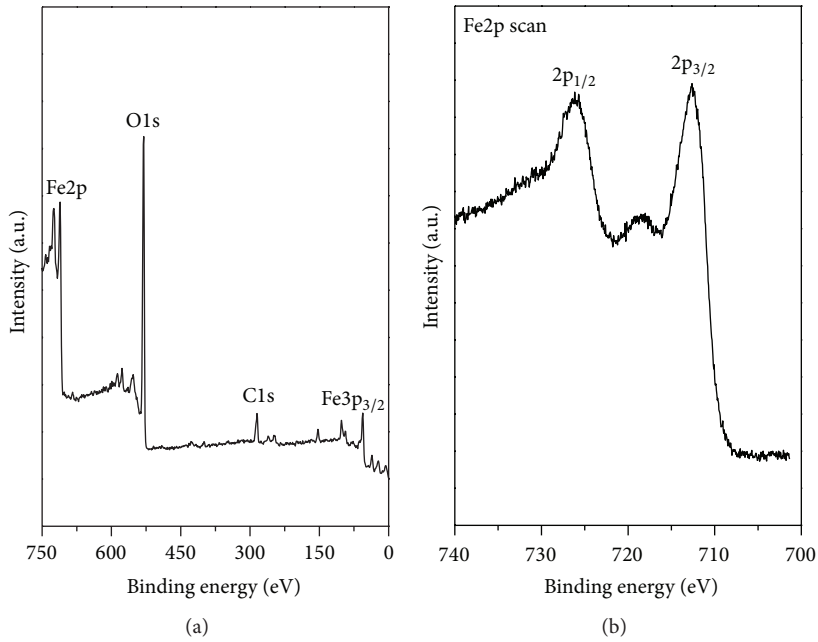

Figure 2: XPS spectra of the prepared porous γ-Fe_2O_3: (a) survey spectrum and (b) high-resolution image of Fe spectrum.

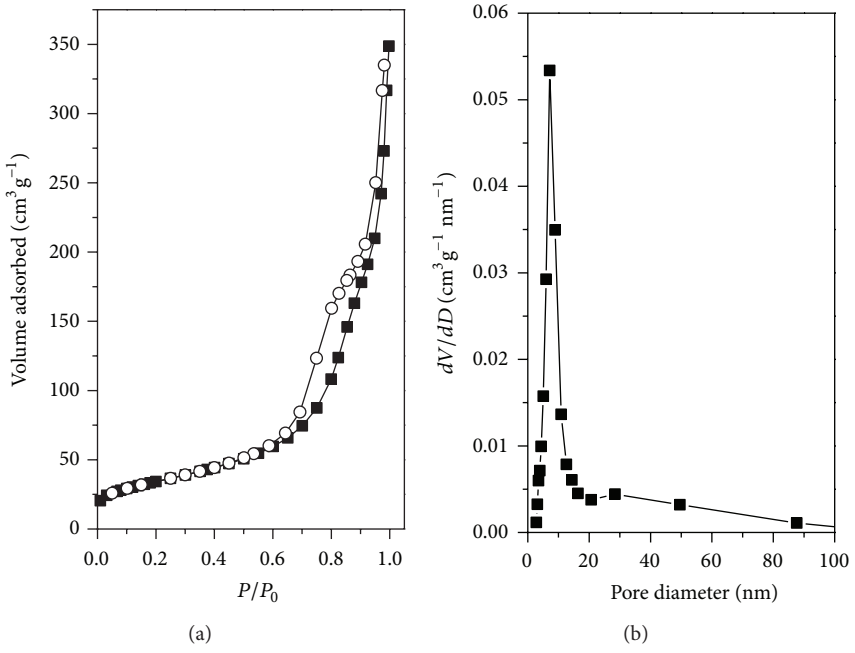

Figure 3: N_2 isotherms (a) and BJH pore size distribution plots (b) of the prepared porous γ-Fe_2O_3.

derived γ-Fe_2O_3 material, with type IV N_2 isotherm at 77 K (Figure 3(a)). This material has a relatively large specific surface area of 123.5 $m^2\ g^{-1}$, which is triple as that of mixed Fe_2O_3 prepared from Prussian blue [32]. Such a high surface area value is presumed to be benefited from the two-step calcination of the template MIL-100(Fe). On the other hand, the pore size distribution (Figure 3(b)) reveals that most of the pores are focused on 10 nm, indicating the mesopores are effective formed for the γ-Fe_2O_3.

The large specific surface area, mesoporous characteristic and high pore volume may offer the obtained γ-Fe_2O_3 as an efficient adsorbent for heavy metal ion removal in water treatment. Figure 4(a) shows a fast uptake rate of As(V) and As(III). It can be seen that the first 30 min corresponds to a rapid adsorption stage for both arsenite and arsenate. The residual concentration of arsenite was less than 40 mg L^{-1} and that of arsenate was less than 20 mg L^{-1} after this fast stage. Thereafter, the adsorption rates decreased and adsorption

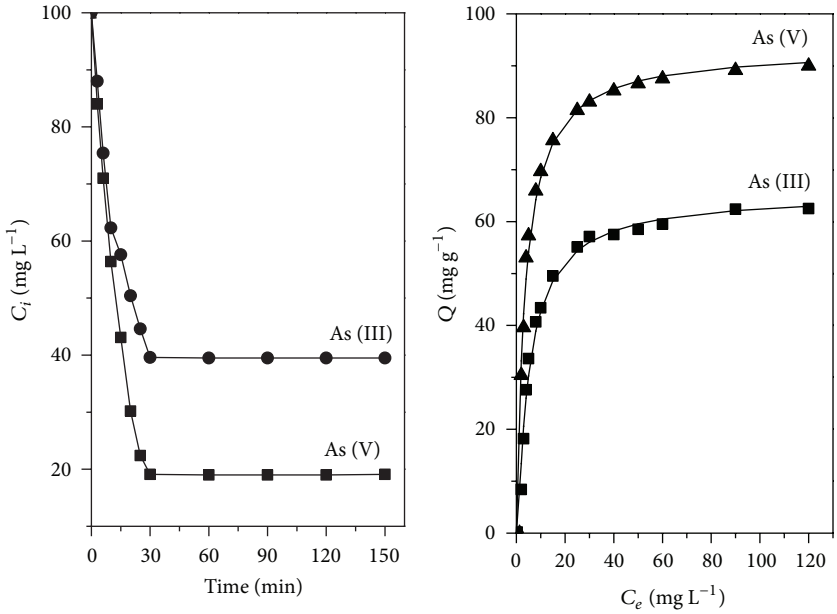

Figure 4: Time-dependent concentration of As(III) (initial concentration of 100 mg L^{-1}) and As(V) (initial concentration of 100 mg L^{-1}) over γ-Fe_2O_3 (a) and adsorption isotherms of As(III) and As(V) on γ-Fe_2O_3.

Table 1: The adsorption capacities of some typical adsorbents.

As(III)		As(V)	
Adsorbent	Adsorption capacity (mg g^{-1})	Adsorbent	Adsorption capacity (mg g^{-1})
γ–Fe_2O_3 nanoparticles [this study]	62.9	γ-Fe_2O_3 nanoparticles [this study]	90.6
Activated carbon [4]	3.1	Titanium dioxide [12]	32.4
Granular iron hydroxide [3]	8.9	Fe-Mn mineral material [13]	14.7
Long-root *Eichhornia crassipes* [5]	1.3	GO-FeOOH [14]	73.2
Zr(IV)-loaded chelating resin [6]	49.1	Chitosan [15]	58.1
Iron oxide-hydroxide [7]	0.475	Fe_2O_3 CAHNs [16]	137.5
γ-Fe_2O_3 nanoparticles [8]	59.2	γ-Fe_2O_3 nanoparticles [17]	50
D-Fe [9]	29.1	γ-Fe_2O_3 flowers [18]	4.75
FeMn synergistic adsorbents [10]	9.3	Fe_3O_4 nanoparticles [19]	46.7
Mg-doped a-Fe_2O_3 nanoadsorbent [11]	10.6	Fe_3O_4 nanoparticles [20]	44.1

equilibrium was reached after 30 min. Adsorption isotherms for these heavy metal ions are plotted in Figure 4(b). The Langmuir model, representing monolayer adsorption, was applied to fit the experimental data according to (1)

$$Q_e = \frac{Q_{max} b C_e}{1 + b C_e}, \quad (1)$$

where Q_{max} is the saturation adsorption capacity of the adsorbent (γ-Fe_2O_3). It is observed that the adsorption could be well described by the Langmuir model ($R^2 > 0.98$) for both As(V) and As(III). The maximal adsorption capacity of the obtained γ-Fe_2O_3 nanoparticles is ca. 62.9 mg g^{-1} for As(III) and 90.6 mg g^{-1} for As(V). Compared to other typical adsorbents reported in the literature, as listed in Table 1, the obtained γ-Fe_2O_3 showed significantly higher adsorption capacities for both of As(V) and As(III). Only Fe_2O_3 CAHNs exhibited a higher adsorption capacity for As(V) than the prepared γ-Fe_2O_3. It should be mentioned that, most results reported in the literature were obtained at the optimized pH value range, thus those high removal capacities may not be achieved at real pH values under the practical conditions. However, the removal capacity values of the obtained γ-Fe_2O_3 were measured without any pH value adjustment in the current work. Thus, the removal capacities obtained here are more indicative of the potential of this material in practical application. Heavy metal ion adsorption by metal oxide is likely due to the combination of static electrical attraction between oxides and heavy metal ions and ion exchange in the aqueous solution [23]. The large specific surface area and porous structure may contribute to the superior performance of the obtained γ-Fe_2O_3.

In summary, porous γ-Fe_2O_3 with large specific surface area, mesoporous characteristic and high pore volume was fabricated via facile solid-state conversion of the as-made MIL-100(Fe) crystal in the current work. When applied as an adsorbent for heavy metal ions removal in wastewater, the obtained γ-Fe_2O_3 nanomaterials show an excellent adsorption performance for As(V) and As(III) ions removal in water treatment.

Conflict of Interests

The authors declare that there is no conflict of interests regarding the publication of this paper.

Acknowledgments

This project was supported by Zhejiang Provincial Natural Science Foundation of China (LY13B030002), Open Research Fund of Top Key Discipline of Chemistry in Zhejiang Provincial Colleges, and Key Laboratory of the Ministry of Education for Advanced Catalysis Materials (Zhejiang Normal University).

References

[1] H. Garelick, A. Dybowska, E. Valsami-Jones, and N. D. Priest, "Remediation technologies for arsenic contaminated drinking waters," *Journal of Soils and Sediments*, vol. 5, no. 3, pp. 182–190, 2005.

[2] L. Dambies, "Existing and prospective sorption technologies for the removal of arsenic in water," *Separation Science and Technology*, vol. 39, no. 3, pp. 603–627, 2004.

[3] B. Daus, R. Wennrich, and H. Weiss, "Sorption materials for arsenic removal from water: a comparative study," *Water Research*, vol. 38, no. 12, pp. 2948–2954, 2004.

[4] C. L. Chuang, M. Fan, M. Xu et al., "Adsorption of arsenic(V) by activated carbon prepared from oat hulls," *Chemosphere*, vol. 61, no. 4, pp. 478–483, 2005.

[5] S. Lin, G. Wang, Z. Na, D. Lu, and Z. Liu, "Long-root *Eichhornia crassipes* as a biodegradable adsorbent for aqueous As(III) and As(V)," *Chemical Engineering Journal*, vol. 183, pp. 365–371, 2012.

[6] T. S. Y. Choong, T. G. Chuah, Y. Robiah, F. L. Gregory Koay, and I. Azni, "Arsenic toxicity, health hazards and removal techniques from water: an overview," *Desalination*, vol. 217, no. 1–3, pp. 139–166, 2007.

[7] P. K. Raul, R. R. Devi, I. M. Umlong, A. J. Thakur, S. Banerjee, and V. Veer, "Iron oxide hydroxide nanoflower assisted removal of arsenic from water," *Materials Research Bulletin*, vol. 49, pp. 360–368, 2014.

[8] S. Lin, D. Lu, and Z. Liu, "Removal of arsenic contaminants with magnetic γ-Fe_2O_3 nanoparticles," *Chemical Engineering Journal*, vol. 211–212, pp. 46–52, 2012.

[9] M. L. Pantoja, H. Jones, H. Garelick, H. G. Mohamedbakr, and M. Burkitbayev, "The removal of arsenate from water using iron-modified diatomite (D-Fe): isotherm and column experiments," *Environmental Science and Pollution Research*, vol. 21, no. 1, pp. 495–506, 2014.

[10] W. Tang, Y. Su, Q. Li, S. Gao, and J. K. Shang, "Mg-doping: a facile approach to impart enhanced arsenic adsorption performance and easy magnetic separation capability to α-Fe_2O_3 nanoadsorbents," *Journal of Materials Chemistry A*, vol. 1, pp. 830–836, 2013.

[11] B. Zhi, H. Ding, D. Wang et al., "Ordered mesoporous MnO_2 as a synergetic adsorbent for effective arsenic(III) removal," *Journal of Materials Chemistry A*, vol. 2, no. 7, pp. 2374–2382, 2014.

[12] S. Bang, M. Patel, L. Lippincott, and X. Meng, "Removal of arsenic from groundwater by granular titanium dioxide adsorbent," *Chemosphere*, vol. 60, no. 3, pp. 389–397, 2005.

[13] E. Deschamps, V. S. T. Ciminelli, and W. H. Höll, "Removal of As(III) and As(V) from water using a natural Fe and Mn enriched sample," *Water Research*, vol. 39, no. 20, pp. 5212–5220, 2005.

[14] F. Peng, T. Luo, L. Qiu, and Y. Yuan, "An easy method to synthesize graphene oxide-FeOOH composites and their potential application in water purification," *Materials Research Bulletin*, vol. 48, no. 6, pp. 2180–2185, 2013.

[15] L. Dambies, "Existing and prospective sorption technologies for the removal of arsenic in water," *Separation Science and Technology*, vol. 39, no. 1–3, pp. 603–627, 2004.

[16] F. Mou, J. Guan, Z. Xiao, Z. Sun, W. Shi, and X. Fan, "Solvent-mediated synthesis of magnetic Fe_2O_3 chestnut-like amorphous-core/γ-phase-shell hierarchical nanostructures with strong As(v) removal capability," *Journal of Materials Chemistry*, vol. 21, no. 14, pp. 5414–5421, 2011.

[17] T. Tuutijärvi, J. Lu, M. Sillanpää, and G. Chen, "As(V) adsorption on maghemite nanoparticles," *Journal of Hazardous Materials*, vol. 166, no. 2-3, pp. 1415–1420, 2009.

[18] L. S. Zhong, J. S. Hu, H. P. Liang, A. M. Cao, W. G. Song, and L. J. Wan, "Self-assembled 3D flowerlike iron oxide nanostructures and their application in water treatment," *Advanced Materials*, vol. 18, no. 18, pp. 2426–2431, 2006.

[19] S. Yean, L. Cong, C. T. Yavuz et al., "Effect of magnetite particle size on adsorption and desorption of arsenite and arsenate," *Journal of Materials Research*, vol. 20, no. 12, pp. 3255–3264, 2005.

[20] S. Zhang, H. Niu, Y. Cai, X. Zhao, and Y. Shi, "Arsenite and arsenate adsorption on coprecipitated bimetal oxide magnetic nanomaterials: $MnFe_2O_4$ and $CoFe_2O_4$," *Chemical Engineering Journal*, vol. 158, no. 3, pp. 599–607, 2010.

[21] J. S. Hu, L. S. Zhong, W. G. Song, and L. J. Wan, "Synthesis of hierarchically structured metal oxides and their application in heavy metal ion removal," *Advanced Materials*, vol. 20, no. 15, pp. 2977–2982, 2008.

[22] W. Jiang, M. Pelaez, D. D. Dionysiou, M. H. Entezari, D. Tsoutsou, and K. O'Shea, "Chromium(VI) removal by maghemite nanoparticles," *Chemical Engineering Journal*, vol. 222, pp. 527–533, 2013.

[23] H. Li, W. Li, Y. Zhang et al., "Chrysanthemum-like α-FeOOH microspheres produced by a simple green method and their outstanding ability in heavy metal ion removal," *Journal of Materials Chemistry*, vol. 21, no. 22, pp. 7878–7881, 2011.

[24] S. C. N. Tang and I. M. C. Lo, "Magnetic nanoparticles: essential factors for sustainable environmental applications," *Water Research*, vol. 47, pp. 2613–2632, 2013.

[25] X. Xu, R. Cao, S. Jeong, and J. Cho, "Spindle-like mesoporous α-Fe_2O_3 anode material prepared from MOF template for high-rate lithium batteries," *Nano Letters*, vol. 12, no. 9, pp. 4988–4991, 2012.

[26] B. Liu, H. Shioyama, T. Akita, and Q. Xu, "Metal-organic framework as a template for porous carbon synthesis," *Journal of the American Chemical Society*, vol. 130, no. 16, pp. 5390–5391, 2008.

[27] F. Meng, Z. Fang, Z. Li et al., "Porous Co_3O_4 materials prepared by solid-state thermolysis of a novel Co-MOF crystal and their superior energy storage performances for supercapacitors," *Journal of Materials Chemistry A*, vol. 1, no. 24, pp. 7235–7241, 2013.

[28] N. Nasihat Sheno, A. Morsali, and S. Woo Joo, "Synthesis CuO nanoparticles from a copper(II) metal-organic framework precursor," *Materials Letters*, vol. 117, pp. 31–33, 2014.

[29] W. Cho, Y. H. Lee, H. J. Lee, and M. Oh, "Multi ball-in-ball hybrid metal oxides," *Advanced Materials*, vol. 23, no. 15, pp. 1720–1723, 2011.

[30] M. Hu, A. A. Belik, M. Imura, K. Mibu, Y. Tsujimoto, and Y. Yamauchi, "Synthesis of superparamagnetic nanoporous iron oxide particles with hollow interiors by using prussian blue coordination polymers," *Chemistry of Materials*, vol. 24, no. 14, pp. 2698–2707, 2012.

[31] L. Zhang, H. B. Wu, S. Madhavi, H. H. Hng, and X. W. Lou, "Formation of Fe_2O_3 microboxes with hierarchical shell structures from metal-organic frameworks and their lithium storage properties," *Journal of the American Chemical Society*, vol. 134, no. 42, pp. 17388–17391, 2012.

[32] L. Zhang, H. B. Wu, R. Xu, and X. W. Lou, "Porous Fe_2O_3 nanocubes derived from MOFs for highly reversible lithium," *CrystEngComm*, vol. 15, no. 45, pp. 9332–9335, 2013.

[33] P. Horcajada, S. Surble, C. Serre et al., "Synthesis and catalytic properties of MIL-100(Fe), an iron(III) carboxylate with large pores," *Chemical Communications*, no. 27, pp. 2820–2822, 2007.

[34] Y. Seo, J. W. Yoon, J. S. Lee et al., "Large scale fluorine-free synthesis of hierarchically porous iron(III) trimesate MIL-100(Fe) with a zeolite MTN topology," *Microporous and Mesoporous Materials*, vol. 157, pp. 137–145, 2012.

[35] J. Shi, S. Hei, H. Liu et al., "Synthesis of MIL-100(Fe) at low temperature and atmospheric pressure," *Journal of Chemistry*, vol. 2013, Article ID 792827, 4 pages, 2013.

[36] B. J. Zhu, X.Y. Yu, Y. Jia et al., "Iron and 1,3,5-benzenetricarboxylic metal–organic coordination polymers prepared by solvothermal method and their application in efficient as(v) removal from aqueous solutions," *The Journal of Physical Chemistry C*, vol. 116, no. 15, pp. 8601–8607, 2012.